Analysis and Application of Quasi-Static and Dynamic Phasor Calculus for Stability Assessment of Integrated Power Electric and Electronic Systems

Jorge Vega-Herrera, Claudia Rahmann, Felipe Valencia, and Kai Strunz

***Abstract*—Power system stability is widely assessed based on tools that rely on the representation of voltages and currents through quasi-static phasor calculus, implying that the network itself and the synchronous machine stators are modeled by algebraic equations. Accordingly, the associated fast transients are neglected, assuming those decay rapidly. However, with the increasing penetration of converter interfaced generation in power systems, the reliance on quasi-static phasor calculus is to be questioned. In this paper, the validity of quasi-static phasor calculus models is verified, and dynamic phasor calculus is considered as the alternative. A methodology to systematically compare quasi-static and dynamic phasor calculus is developed. It includes frequency response, modal, and sensitivity analyses. The methodology is applied to an IEEE test network considering penetrations of converter interfaced generation of up to 100%. The models are implemented in MATLAB. The H-infinity norm is proposed as an indicator to identify differences in the applicability of the models. The results show that the quasi-static phasor calculus is suitable for stability analysis only if low bandwidths of converter controls are given. Dynamic phasor calculus instead is suitable and applicable to generic stability studies of integrated power electric and electronic systems with high penetration of renewables.**

***Index Terms*—Dynamic phasor, quasi-static phasor, system stability, system modeling and simulation, power electronics.**

I. Introduction

FOR almost a century, stability has been recognized as one of the key issues to be dealt with in order to achieve a secure power system operation [1]. For the assessment of diverse stability issues, the study of power system transients is of interest. In Fig. 1 the time scales of transient phenomena relevant to power system analysis are shown. The time scales range cover the wide spectrum of wave phenomena, electromagnetic transients, electromechanical transients, and up to thermodynamic phenomena [2]. Depending on the nature of the transients considered for particular stability studies, dedicated assumptions on component modeling are to be made. Thus, the system is represented at a respective and appropriate degree of detail for the limited bandwidth of transients under study.

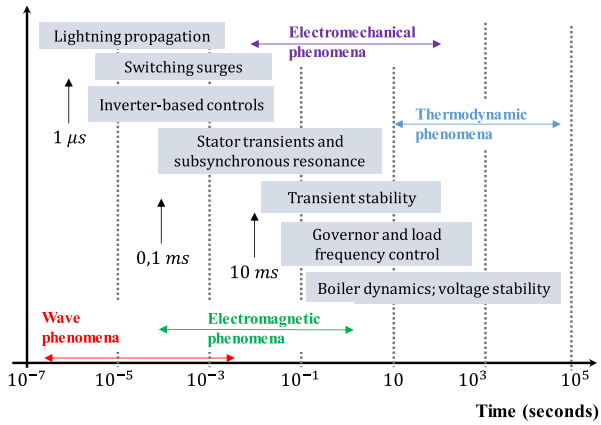

Fig. 1. Different time scales of power systems transients [15].

In power systems dominated by synchronous generators (SG), the main focus for stability assessments has traditionally been on the time scale of electromechanical or slower phenomena, as indicated in Fig. 1. The time scale of electromechanical phenomena is shown to range from several milliseconds to seconds. The oscillation frequencies of the associated transients are typically between 0.1 Hz and 5 Hz [3]–[5]. The concentration on those frequencies has allowed several modeling simplifications, which in turn led to the well-known stability assessments based on quasi-static phasor calculus (QPC) [3]. When using QPC, the behavior of the electric network is described by a set of algebraic equations, in which electromagnetic transients are neglected. This is justified because the decay of electromagnetic transients associated with the network is comparatively fast, and therefore has been little justification to include their effects in system stability studies.

Nevertheless, the increase in the penetration of converter interfaced generation (CIG) has considerable changed the nature of transients in power systems due to the fast response times

Manuscript received November 30, 2019; revised April 3, 2020 and August 17, 2020; accepted September 27, 2020. Date of publication October 12, 2020; date of current version April 19, 2021. This work was supported by the Chilean National Agency for Research and Development, ANID/FONDECYT/11160228, ANID/Fondap/15110019, ANID/21161139, Energy Program ANID/Ministry of Energy. In addition, the authors gratefully acknowledge Project EchtEWende (n° 03ET4060), funded by the German Federal Ministry for Economic Affairs and Energy (BMWi). Paper. no. TPWRS-01803-2019. *(Corresponding author: Claudia Rahmann.)*

Jorge Vega-Herrera is with the Electrical Engineering Department, University of Antofagasta, Antofagasta, Chile (e-mail: jorge.vega.herrera@gmail.com).

Claudia Rahmann is with the Electrical Engineering Department, University of Chile, Santiago, Chile (e-mail: crahmann@ing.uchile.cl).

Felipe Valencia is with the Electrical Engineering, Universidad de Chile, Santiago 8320000, Chile (e-mail: felipe.valencia@gmail.com).

Kai Strunz is with the Elektrotechnik und Informatik, Technische Universität Berlin, Berlin, Berlin 10587, Germany (e-mail: kai.strunz@tu-berlin.de).

Color versions of one or more of the figures in this article are available online at https://ieeexplore.ieee.org.

Digital Object Identifier 10.1109/TPWRS.2020.3030225

of CIG [6]–[8]. This can be seen from Fig. 1, where the time scale related to the inverter-based controls varies from few microseconds to several milliseconds. This time scale is actually related to electromagnetic phenomena, thus being much faster than the electromechanical phenomena of oscillations of SG. Accordingly, the transients of power systems dominated by CIG become faster, thereby leading to new control interactions and stability issues [9]–[12]. Among the key instability drivers in CIG are their control loops with fast response times such as the phase-lock-loop (PLL) controllers [9], [10] and inner current loop controllers [9], [13]. Although recent studies have shown that these control loop instabilities are more likely to arise in weak networks with low levels of inertia, they may also appear in case of power systems with lower levels of CIG, depending on system operating conditions [14].

Considering the stability assessment of power systems, the fast response times of CIG are expected to considerably extend the bandwidth of relevant transients towards the electromagnetic time scale. Accordingly, the modeling simplifications in QPC models need to be questioned. This means that fast phenomena related to the network and fast response devices must not be further neglected [16]. Indeed, according to [17], the fast transients of power electronics converters may invalidate the typical time scale separation approach used in stability assessments.

While some recent studies have addressed different stability issues in presence of CIG [9]–[12], what is still missing is a scientific foundation for the modeling, analysis, and control of power systems dominated by CIG [17]. In particular, given the fact that fast phenomena of CIG extend the bandwidth of relevant transients for stability studies, the question of how this affects the validity of using QPC-based models for evaluation stability remains unanswered [8], [18], [19]. However, with the rise of CIG, users of simulation tools and power system planners urgently need the answer. To address this issue, a comprehensive and systematic comparative study is performed, in which dynamic phasor calculus (DPC) [20] is considered as alternative to QPC. In DPC, the electric network is described through a set of differential rather than algebraic equations, thus being more accurate than QPC models [20]–[26]. DPC-based models have been applied to simulate a broad range of transients in different systems, including unbalanced distribution systems [27], microgrids [25], transients of electric machines [20], [28], and power electronic systems [26], [29], [30]. In all these applications, DPC-based models have demonstrated a good performance for representing the transients under study.

The fundamental contributions in this paper are threefold. First, a methodology for a systematic comparative analysis of QPC and DPC is developed. The methodology covers a sequence of stages where a set of indicators and criteria is defined. The sequence of the stages enables the identification of critical CIG control system parameters that have a significant influence on the accuracy of models based on QPC. Thus, the validity range of QPC can be clearly identified. Furthermore, the stages make uses of well-accepted analysis techniques, which is of significant practical value. Thus, the methodology can be directly applied by power system planners to identify the validity of QPC-based models for their particular network conditions.

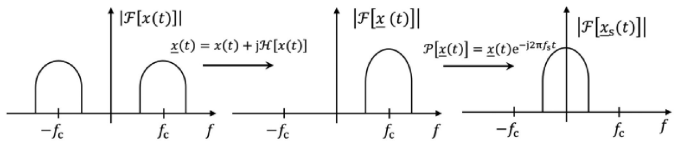

Fig. 2. Application of Hilbert transformation and shifting by carrier frequency.

Second, the methodology is applied to a modified IEEE test network for a broad range of CIG penetration levels, including the level of 100%. Besides determining the validity of QPC models, the application of the methodology is enriched with an analysis of the limitations associated with QPC models. The results obtained are validated through electromagnetic transient (EMT) simulations wherein the switching of power electronic devices used in CIG are modeled. Third, for power systems with CIG, the validity ranges of models based on QPC and DPC are identified.

In Section II, the use of phasors in power systems is reviewed. The proposed methodology for the comparative analysis is given in Section III. In Section IV, the test network used is presented. Finally, the results are discussed in Section V, and the conclusions are drawn in Section VI.

II. Phasor Calculus in Power Systems

A. Dynamic Phasor Calculus

During normal operation, voltages and currents of power systems are rather balanced three-phase sinusoidal signals with a system frequency $f_c = 50$ Hz or $f_c = 60$ Hz, respectively. During low-frequency perturbations, power systems experience low-frequency transients. In the frequency domain, they are characterized by a bandpass characteristic centered on f_c. The latter can be considered as the carrier frequency. This bandpass characteristic is displayed in Fig. 2, where the signal $x(t)$ can be a voltage or a current signal [21], [24]. From the figure, it can be seen that the Fourier spectrum $|\mathcal{F}[x(t)]|$ is symmetric to the axis $f = 0$ Hz. Accordingly, the negative frequency components of the spectrum do not provide further information about the real signal $x(t)$.

The analytic signal $\underline{x}(t)$ of the real signal $x(t)$ is defined as follows [31]:

$$\underline{x}(t) = x(t) + \mathrm{j}\mathcal{H}[x(t)] \tag{1}$$

where the underscore indicates that $\underline{x}(t)$ is complex, and $\mathcal{H}[.]$ is the Hilbert transform, which is formally defined as:

$$\mathcal{H}[x(t)] = \frac{1}{\pi} \int_{-\infty}^{\infty} \frac{x(\tau)}{t-\tau} \mathrm{d}\tau \tag{2}$$

The resulting Fourier spectrum $|\mathcal{F}[\underline{x}(t)]|$ now only extends to positive frequencies as also shown in Fig. 2.

An analytic signal can be shifted by the shift frequency f_s as follows:

$$\underline{x}_s(t) = \mathcal{P}[\underline{x}(t)] = \underline{x}(t)\, \mathrm{e}^{-\mathrm{j}2\pi f_s t} \tag{3}$$

In power systems, it is of major interest to set the shift frequency $f_s = f_c$ of 50 Hz or 60 Hz. The new signal $\underline{x}_s(t)$ then appears as a dynamic phasor, and its frequency spectrum changes as shown in Fig. 2. The shifted signal behaves as a low-pass signal, whose maximum frequency is reduced due to the shifting. As a result, a lower sampling rate can be used to simulate the transients using dynamic phasor signal $\underline{x}_s(t)$ compared with the natural bandpass signal $x(t)$. In general, the shifted-frequency formulation (3) of the dynamic phasor is also applicable to the modeling of transients at high frequencies beyond those suggested by Fig. 2, as long as a sufficiently small time-step size is chosen [21].

The original signal can be reconstructed through the reverse process:

$$x(t) = \mathrm{Re}\left[\underline{x}_s(t)\, e^{j2\pi f_s t}\right] \tag{4}$$

The transient simulation also involves the numerical solution of a set of differential and algebraic equations (DAE). To obtain the DAE using DPC, the derivative of $\underline{x}_s(t)$ is to be known. Deriving the analytical signal $\underline{x}(t)$ described in (3) and defining $\omega_s = 2\pi f_s$ yields:

$$e^{-j\omega_s t}\frac{d\underline{x}(t)}{dt} = \frac{d\underline{x}_s(t)}{dt} + j\omega_s \underline{x}_s(t) \tag{5}$$

B. Quasi-Static Phasor Calculus

In order to obtain a model based on QPC from a model based on DPC, we consider a differential equation that describes the relationship between the two analytic signals $\underline{x}(t)$ and $\underline{y}(t)$:

$$k\frac{d\underline{x}(t)}{dt} = \underline{y}(t) \tag{6}$$

Both quantities are supposed to have a Fourier spectrum similar to the one as shown in the center of Fig. 2. Using (5) to calculate the derivative of an analytical signal, (6) can be expressed by DPC as follows [3]:

$$k\left[\frac{d\underline{x}_s(t)}{dt} + j\omega_s \underline{x}_s(t)\right] = \underline{y}_s(t) \tag{7}$$

The QPC model is then obtained by setting $\frac{d\underline{x}_s(t)}{dt} = 0$ in (7). This results in the algebraic equation:

$$jk\omega_s \underline{x}_s(t) = \underline{y}_s(t) \tag{8}$$

By neglecting the derivatives from (7), it is assumed that the transient response of the state variable $\underline{x}_s(t)$ is fast with respect to the time scale of interest in the particular study. In the literature, this model reduction process is known as singular perturbation theory [32]. This theory has been successfully applied within stability studies for neglecting transients in the stator fluxes and electric networks [33].

A representation of a signal based on QPC yields a suitable approximation if the transients of interest involve small values of $\frac{d\underline{x}_s(t)}{dt}$. This is actually the case when the relevant transients are slow rotor electromechanical oscillations of SG, which cause small frequency deviations from the system frequency f_c in electric quantities such as voltages and currents. The bandwidth of frequencies of these transients ranges from 0.1 Hz to 5 Hz [1], [3], [5].

TABLE I
COMPARISON OF RLC REPRESENTATION

Circuit element	DPC	QPC
R	$\underline{v}_{Rs} = R\underline{i}_{Rs}$	$\underline{v}_{Rs} = R\underline{i}_{Rs}$
L	$\underline{v}_{Ls} = L\frac{d\underline{i}_{Ls}}{dt} + j\omega_s L\underline{i}_{Ls}$	$\underline{v}_{Ls} = j\omega_s L\underline{i}_{Ls}$
C	$\underline{i}_{Cs} = C\frac{d\underline{v}_{Cs}}{dt} + j\omega_s C\underline{v}_{Cs}$	$\underline{i}_{Cs} = j\omega_s C\underline{v}_{Cs}$

C. Basic Models of RLC Components

In this section, we briefly compare the DPC and QPC for describing the basic elements of an electrical circuit. The following equation defines the transients for an inductance:

$$L\frac{d\underline{i}_L(t)}{dt} = \underline{v}_L(t) \tag{9}$$

Applying (7) to (9), the model of the inductance based on DPC is as follows:

$$L\frac{d\underline{i}_{Ls}(t)}{dt} + j\omega_s L\underline{i}_{Ls}(t) = \underline{v}_{Ls}(t) \tag{10}$$

The QPC model of the inductance is then obtained by neglecting the derivative of the DPC model:

$$j\omega_s L\underline{i}_{Ls}(t) = \underline{v}_{Ls}(t) \tag{11}$$

Proceeding similarly, the models of the resistor and capacitor can also be obtained. A summary of the models using DPC and QPC is shown in Table I.

III. PROPOSED METHODOLOGY

As mentioned in the introduction, this work relies on the assumption that an increase of CIG in power systems extends the bandwidth of relevant transients for stability assessments towards faster electromagnetic time scales. Considering this, the objective is to methodically determine how this extended bandwidth modifies the validity range of QPC-based models. To answer this, we propose the methodology depicted in Fig. 3, in which DPC-based models are considered as alternative to QPC-based models. The methodology establishes a set of procedures and evaluation criteria to perform a systematic comparison between both modeling techniques. The methodology makes use of a simulation-based approach. Compared to a system-theoretic analytic approach, the main advantage of simulation-based approaches is that they are less restricted by modeling limitations, thus allowing to obtain more accurate results [17]. The application of a wide range of penetration levels of CIG enhances the confidence in the results.

The methodology is organized into five stages. A key contribution resides in the proposed sequence of steps. In this context, it is of significant practical value that the stages make use of recognized and well-accepted simulation and analysis techniques. As such, the methodology can be used by power system planners to clearly identify the validity of simulation

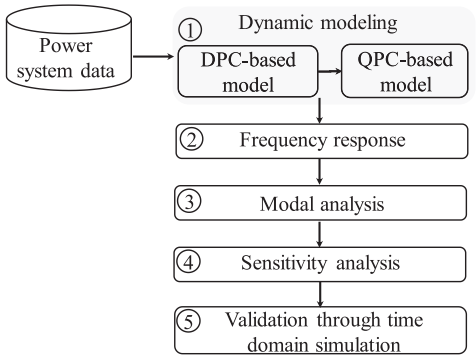

Fig. 3. Sequence of stages of proposed methodology.

techniques for their particular and individual network situation. Given the large size of investments made into grid extension and modification for ensuring stability when integrating CIG, the knowledge on how to relate the choice of simulation tools with the quantity of CIG penetration levels is very important in order to prevent costly misjudgments.

A. Stage 1: Dynamic Modeling

In the first stage of the methodology, models for the system under study considering DPC and QPC techniques are to be obtained. Regarding the DPC-based model, in the case of SG with steam turbines, an eighth-order model is used, whereas a seventh-order model is used for SG with hydraulic turbines [4]. In both cases, standard models for governors and automatic voltage regulators are included [34], [35]. For CIG, an average voltage source converter (VSC) model where the switching transients are neglected is considered [29], [36], [37]. In this model, the transient behavior of the CIG is determined mainly by its control loops. These control loops are represented in a rotational dq references frame [38]. The loops are composed of an outer voltage control loop, an inner current control loop, and the phase-locked loop (PLL). The PLL is used to estimate the phase angle of the voltage at the point of common coupling. The phase angle is used to transform abc to dq signals and then to control the CIG [39]. The CIG control systems applied are generic and commonly used for simulation of transients [40]–[42].

The lines are modeled using π equivalent circuits with lumped parameters and transformers through series RL circuits. Loads are modeled as constant impedances, which are series RL circuits. These models have been recommended for assessing electromechanical transients and control interactions between CIG and power systems [43]–[46].

Combining the models of all power system components, a DPC-based model of the form shown in (12) is obtained. In (12), $\boldsymbol{x}$, $\boldsymbol{z}$, $\boldsymbol{u}$, and $\boldsymbol{y}$ represent the vectors of the state variables, variables related to the algebraic equations, inputs, and outputs respectively [47].

$$\begin{aligned} \dot{\boldsymbol{x}} &= \boldsymbol{f}(\boldsymbol{x}, \boldsymbol{z}, \boldsymbol{u}) \\ \mathbf{0} &= \boldsymbol{g}(\boldsymbol{x}, \boldsymbol{z}, \boldsymbol{u}) \\ \boldsymbol{y} &= \boldsymbol{h}(\boldsymbol{x}, \boldsymbol{z}, \boldsymbol{u}) \end{aligned} \tag{12}$$

TABLE II
SUMMARY OF POWER SYSTEM MODELS

Component	References		Quantities neglected in QPC-based models
	DPC	QPC	
Synchronous generator	[4]	[2]	Derivatives of the stator flux linkages
Transmission networks, Transformers, and loads	[16]	[2]	Derivatives of the voltages in capacitors and derivatives of the currents in inductors.
CIG current control and coupling inductance	[40]	[40]	Derivatives of the current in the coupling inductance.
CIG PLL	[50]	[50]	-
CIG outer voltage control	[41]	[41]	-

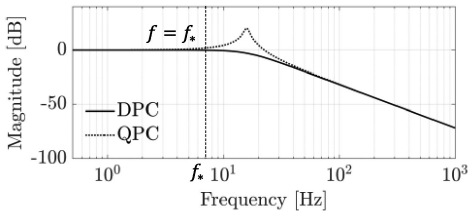

Fig. 4. Illustrative Bode plot for comparing DPC and QPC-based models.

Upon completion of the DPC-based model, the QPC-based model is derived by neglecting some derivatives in (12). The derivatives to be neglected can be selected mainly by two approaches: based on physical system understanding and manual reduction [9], [42], [48] or based on singular perturbation theory [32]. By neglecting the derivatives, it is assumed that the transients of the related state variables decay rapidly, and therefore there would be little justification for including their effects in stability studies [4]. This has been actually the case for the stator flux linkages of SG, the voltages in capacitances, and the currents in inductances of transmission networks of power systems dominated by synchronous machines. Hence, their derivatives have been set to zero in stability assessments based on QPC [3], [4]. By neglecting the derivatives of the selected state variables, some differential equations in (12) become algebraic. Table II shows the references used in modeling each component considered in this paper and the quantities neglected for each component. A detailed description of each component model is presented in [49].

B. Stage 2: Frequency Response

Once the DPC and QPC-based models of the power system are completed, the steady-state frequency responses of both models are compared in the second stage for different levels of CIG. The objective is to identify the lowest frequency f_* at which the magnitudes of the frequency responses differ by a given threshold ϵ. This allows us to determine the frequency bandwidth in which QPC-based models are still suitable for representing the system transients as a function of the CIG level. The frequency f_* is obtained from a Bode diagram as illustrated in Fig. 4.

C. Stage 3: Modal Analysis

The third stage of the methodology is dedicated to modal analysis using small-signal linearization around the steady-state operating point for both models. The objective is to analyze the modes that involve oscillations with frequencies higher than f_* and to determine the relevant state variables for different levels of CIG. We mainly focus on the modes with frequencies higher than f_* because those are in the region where differences between both modeling techniques become pronounced as found in Stage 2. These modes with frequencies higher than f_* are actually those that may lead to inaccurate results when using QPC-based models. The state variables related to these modes are identified through the analysis of participation factors [4].

To quantitatively compare the dynamic performance for both linearized models, we use the H-infinity norm $\mathcal{H}_\infty$. For a MIMO (multiple inputs multiple outputs) system described by $\dot{\boldsymbol{x}}\,(t) = \boldsymbol{A}\boldsymbol{x}(t) + \boldsymbol{B}\boldsymbol{u}(t)$, $\boldsymbol{y}\,(t) = \boldsymbol{C}\boldsymbol{x}(t) + \boldsymbol{D}\boldsymbol{u}(t)$, and with a transfer matrix $\boldsymbol{G}\,(s) = \boldsymbol{C}(s\boldsymbol{I} - \boldsymbol{A})^{-1}\boldsymbol{B} + \boldsymbol{D}$, the H-infinity norm can be defined as follows [47], [51], [52]:

$$\|\boldsymbol{G}\,(s)\,\|_\infty \triangleq \max_{\boldsymbol{u}(t)\neq 0} \frac{\|\boldsymbol{y}\,(t)\,\|_2}{\|\boldsymbol{u}\,(t)\,\|_2} \tag{13}$$

$$\|\boldsymbol{y}\,(t)\,\|_2 = \left(\int_0^\infty \boldsymbol{y}^{\mathrm{T}}\,(t)\,\boldsymbol{y}\,(t)\,\mathrm{d}t\right)^{\frac{1}{2}} \tag{14}$$

$$\|\boldsymbol{u}\,(t)\,\|_2 = \left(\int_0^\infty \boldsymbol{u}^{\mathrm{T}}\,(t)\,\boldsymbol{u}\,(t)\,\mathrm{d}t\right)^{\frac{1}{2}} \tag{15}$$

The value of $\|\boldsymbol{G}\|_\infty$ represents the maximum root-mean-square gain of the system for any direction of the input vector. If the system has all the eigenvalues in the left half of the complex plane, the small-signal model is stable and $\|\boldsymbol{G}\|_\infty$ is bounded. If $\|\boldsymbol{G}\|_\infty$ is not bounded, the small-signal model is unstable or has poles on the imaginary axis. Therefore, as the $\|\boldsymbol{G}\|_\infty$ increases, the system becomes less damped. Hence, if the QPC-based model has a noticeably different value of $\|\boldsymbol{G}\|_\infty$ compared with its counterpart based on DPC, then the results obtained with the QPC-based model are less accurate because the dynamic performance has become significantly different due to the simplifications made. The aforementioned simplifications are those presented in Table II.

D. Stage 4: Sensitivity Analysis

The next stage consists in performing a sensitivity analysis of key system parameters. This allows to verify if the observations of Stage 3 are plausible even when relevant parameters of the system change. The parameters are selected according to the relevant state variables, which are defined from the analysis of the participation factors in Stage 3. Once the key parameters have been selected, we define a range of variations of these parameters based on typical values used in transient studies and repeat the analysis specified in Stage 3.

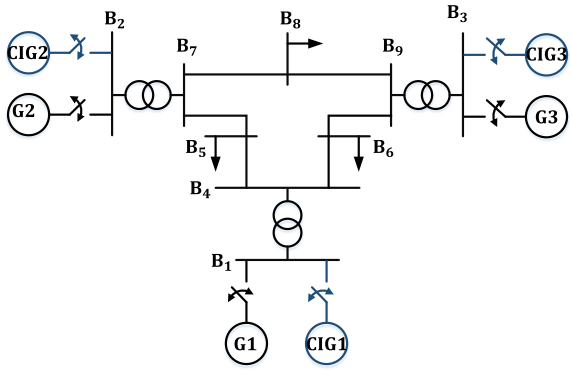

Fig. 5. IEEE-9 bus system with switches to adapt generation portfolio [54].

TABLE III
MAIN CHARACTERISTICS OF SYNCHRONOUS GENERATORS

Properties	G1	G2	G3
Type	Hydro	Steam	Steam
Rated power [MVA]	247.5	192	128
Inertia constant [s]	9.6	3.3	2.4
Rated voltage [kV]	16.5	18	13.8

E. Stage 5: Validation Through Time Domain Simulation

In this stage, we perform simulations of transients. We verify and validate all relevant observations of the previous stages and draw main conclusions. For this purpose, we simulate a system disturbance using DPC, QPC, and EMT modeling techniques. EMT simulations in abc phase variables are performed in PSCAD [28], [53] to verify the accuracy of DPC models. Finally, the time series of selected system variables are compared.

IV. DESCRIPTION OF POWER SYSTEM IMPLEMENTED

The used IEEE 9-bus system, as shown in Fig. 5 [54], is extended by a set of configuration switches to allow for the study of various generation portfolios. The system has three SG at 60 Hz, two with steam turbines, G2 and G3, as well as one with a hydraulic turbine, G1. The characteristics of these generators are summarized in Table III. We consider a load of 315 MW with 0.94 lagging power factor and system parameters as given in [54]. The load is equivalent to 56% of the total rated generation capacity.

To compare DPC and QPC-based models, two CIG units are added at buses B1 and B3. The capacities of CIG1 and CIG3 are the same as for the generators G1 and G3, respectively. For the 100% of CIG level, the generator G2 is replaced by the CIG2 unit operating in grid forming mode as a virtual synchronous generator [55]. The capacity of CIG2 is equal to generator G2 and the synthetic inertia of CIG2 is equivalent to the inertia of generator G2. Table IV summarizes the dispatch for different generator portfolios. When the power of a generator is shown to be zero, then the connector switch related to the generator is open. Table IV also includes the system inertia H_{sys}, which is defined as [4]:

$$H_{\mathrm{sys}} = \frac{\sum_{i=1}^{n} H_i S_i}{\sum_{i=1}^{n} S_i} \tag{16}$$

TABLE IV
DISPATCH AND SYSTEM INERTIA FOR DIFFERENT GENERATOR PORTFOLIOS

CIG Levels [%]	G1 [MW]	G2 [MW]	G3 [MW]	CIG1 [MW]	CIG2 [MW]	CIG3 [MW]	H_{sys} [s]
0	163	77	80	0	0	0	5.82
35	0	91	120	55	0	55	1.66
70	0	98	0	110	0	110	1.13
100	0	0	0	189	4	126	1.13

TABLE V
CONTROL SYSTEM PARAMETERS OF CIG1 AND CIG3 UNITS

Properties	Value
Proportional gain of current controller k_{p}	0.40
Integral gain of current controller k_{i}	90.00
Proportional gain of PLL controller k_{pPLL}	101
Integral gain of PLL controller k_{iPLL}	2562
Time constant of voltage measure T_{r} $[s]$	0.05
Proportional gain of reactive power controller k_{pq}	5.00
Integral gain of reactive power controller k_{iq}	0.50

where H_i, S_i, and n respectively denote the inertia constant, the rated power of the generator, and the number of generators connected to the system contributing a finite inertia. Since the CIG2 operates as a virtual synchronous generator, its synthetic inertia is also included for calculating the system inertia. This explains the unchanged values of H_{sys} in rows three and four of the table.

The SG are modeled as given in Section III-A and Table II [4]. All generators are equipped with a voltage regulator of type DC1A IEEE [34]. The governor of the steam turbines is of type IEEE TGOV1, while the hydraulic turbine is of type IEEE HYGOV [35]. The models of the CIG1 and CIG3 units include the control systems described in Table II. The parameters of the current control loop are chosen in order to get a settling time of 20 ms, which is a typical value used in simulations with power converters [42], [56]. The PLL control has a bandwidth of 20 Hz [39]. The control parameters of the CIG1 and CIG3 units are summarized in Table V. In the case of QPC-based models, G2 and G3 models are of sixth order, and G1 is a fifth-order model because the stator flux linkage transients are neglected [2]. The control systems of the SG are kept identical to those used for the DPC-based models.

As mentioned in Section III-E, the accuracy of DPC models, is verified by performing EMT simulations in PSCAD. For these simulations, distributed-parameter transmission lines models are used. The VSC configuration considered in CIG is the two-level three-phase VSC. In order to represent high-frequency switching transients due to pulse width modulation (PWM) control, the switching function model of the VSC converter described in [38] is used. The PWM compares a high-frequency triangular carrier signal with a modulating signal with a lower frequency. The models of transformers, loads, SGs with their control systems, and the control systems of CIG are kept identical to those used in DPC models.

The test system using DPC and QPC was implemented in MATLAB/Simulink. To carry out the frequency response and modal analysis, the system was linearized using the Linear Analysis Tool from MATLAB/Simulink [57]. For the frequency response analysis, the "bode" function of MATLAB was used. We considered as input signal the reference power and as output signal the angular electrical frequencies of the generators. The relations are chosen because in a power system with low inertia the frequency control is one of the main challenges [58].

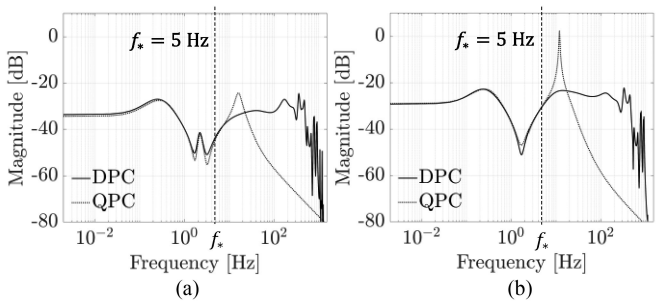

Fig. 6. Magnitude of Bode plot; a) 35% of CIG, b) 70% of CIG.

V. COMPARATIVE ANALYSIS OF DPC AND QPC

A. Frequency Response Analysis

The Bode diagrams of the system when considering 35% and 70% of CIG penetration are depicted in Fig. 6. The considered input signal is the reference power of the generator connected at B3, $P_{\mathrm{B3}}^{\mathrm{ref}}$. The output signal is the angular electrical frequency at bus B1, $\omega_{\mathrm{B1}}^{\mathrm{elec}}$. The frequency f_* from which on the simulations based on DPC and QPC differ was determined considering a tolerance of $\epsilon = 5\%$.

Fig. 6 shows that the maximum frequency up to which both models give a similar frequency response is $f_* \approx 5$ Hz. For CIG levels higher than 35% G3 is disconnected. In such configurations, the system modeled by QPC shows a resonance close to 12 Hz, whereas the DPC-based model does not show such behavior. This suggests that QPC-based models become less accurate if the frequency of the transients of interest adopts values beyond 5 Hz. The frequency range in which both models give a similar frequency response, coincides with the frequency range related to slow rotor oscillation of electric machines, which typically varies between 0.1 Hz and 5 Hz. In the DPC-based models, the rapid changes of magnitudes observed for frequencies higher than 500 Hz are mainly since the network is modeled by differential rather than just algebraic equations (as shown in Table II). In these frequency ranges, the outputs are very well attenuated because the gain of the transfer function is lower than – 40 dB. Therefore, their relative impact on the transfer function compared with those of other frequency ranges is low. Qualitatively, similar observations are made at other penetration levels of CIG. The frequency f_* is also retained for further input-output combinations.

B. Modal Analysis

As it was described in Stage 3 of the methodology, the modal analysis is focused on modes with frequencies higher than f_* as those modes are expected to have a detrimental effects on

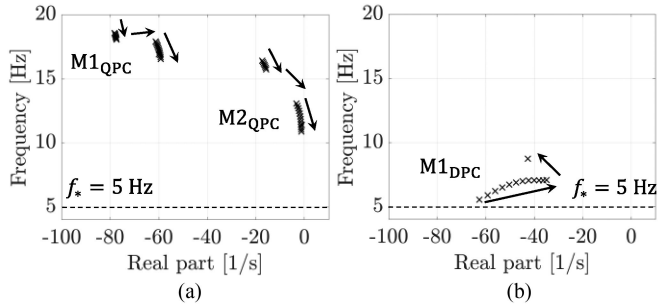

Fig. 7. Eigenvalue loci of the modes related to the CIG control systems for CIG levels between 5 and 100%; a) QPC-based model, b) DPC-based model.

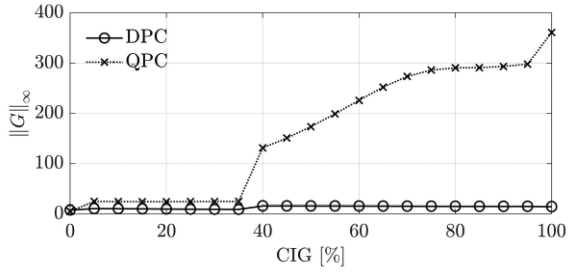

Fig. 8. $\|\boldsymbol{G}\|_\infty$ as a function of CIG level.

accuracy of QPC. In these frequency range, the system modeled using QPC has two modes of oscillation, hereafter identified by $\mathrm{M1_{QPC}}$ and $\mathrm{M2_{QPC}}$, respectively. The analysis of participation factors reveals that the modes $\mathrm{M1_{QPC}}$ and $\mathrm{M2_{QPC}}$ are pertaining to the control systems of the CIG1 and CIG3 units. These modes are mainly related to the state variables of the current control loops and the PLL of those CIG units.

In Fig. 7, the effect of the penetration levels of CIG on the eigenvalues corresponding to the modes $\mathrm{M1_{QPC}}$ and $\mathrm{M2_{QPC}}$ is shown. The root loci reveal a reduction in damping as CIG level rise. However, the mode $\mathrm{M1_{QPC}}$ still remains well damped for all the penetration levels, with its oscillation frequency moving from 18 Hz to 16 Hz. Its lowest damping ratio is 49% for the case of a CIG level of 100%. On the other hand, the mode $\mathrm{M2_{QPC}}$ becomes poorly damped as the CIG level grows. The damping ratio changes from 16% to 1.3%, and the oscillation frequency moves from 16 Hz to 11 Hz. The decrease in the damping ratio is accentuated when the CIG levels exceed 35%. This is because generator G3 is then disconnected from the system, leading to a reduced system inertia, as Table IV shows.

Given the above, the modal analysis performed when the system is modeled by QPC suggests a poor dynamic performance at high levels of CIG. Moreover, QPC analysis suggest that the system is close to loosing small-signal stability.

The system modeled using DPC has high, medium, and low frequency oscillation modes. We can categorize these modes into the following frequency ranges: 400 Hz to 1500 Hz, 60 Hz to 400 Hz, and 0 Hz to 60 Hz, respectively. For high frequency modes, the analysis based on the participation factors shows that these modes are related to electromagnetic transients pertaining to the transmission network, the stator fluxes of the SG, and the CIG control. Dominant state variables are not observed in the high frequency modes. Some of these modes have low damping ratios. However, as it was shown in the frequency response analysis, for frequencies higher than 500 Hz, the outputs are very well attenuated. Therefore, the high frequency modes are not critical for the small-signal stability of the system. This observation was also reported in [45]. For medium frequency modes, participation factor analysis shows that they are related to the electric network. The state variables are mainly related to the transmission network, and they are well damped. Both high and medium frequency modes are not significantly affected by the level of CIG.

The critical difference between QPC and DPC modeling techniques appears for the low frequency modes and particularly in the modes associated with the control system of the CIG1 and CIG3 units. In the system modeled using DPC, there are four modes related to the CIG, $\mathrm{M1_{DPC}}$, $\mathrm{M2_{DPC}}$, $\mathrm{M3_{DPC}}$, and $\mathrm{M4_{DPC}}$, respectively. The participation factor analysis reveals that the mode $\mathrm{M1_{DPC}}$ is mainly related to the state variables of the current control loops and the PLL of CIG. The mode $\mathrm{M1_{DPC}}$ is the only mode related to the CIG control for which its corresponding eigenvalue appears in the same complex plane area as the eigenvalues of the modes $\mathrm{M1_{QPC}}$ and $\mathrm{M2_{QPC}}$. This can be recognized in Fig. 7. For all levels of CIG, the mode $\mathrm{M1_{DPC}}$ is well damped, taking a minimum value of 61% for damping. In the cases of the modes $\mathrm{M2_{DPC}}$, $\mathrm{M3_{DPC}}$, and $\mathrm{M4_{DPC}}$, the state variables that have high participation are related to the current control loop and the filter of CIG. The level of CIG does not affect these modes significantly. In fact, they are always well damped with damping ratios higher than 70%. Given the above observations, the modal analysis performed on the system modeled by DPC suggests that the linearized system is stable regardless of the penetration level of CIG. In addition, it has better dynamic performance compared with its counterpart based on QPC.

Fig. 8 shows the H-infinity norm $\|\boldsymbol{G}\|_\infty$ for different levels of CIG. As the CIG increases, there are no significant variations in the $\|\boldsymbol{G}\|_\infty$ when the system is modeled using DPC. However, in the case of the QPC-based model, the $\|\boldsymbol{G}\|_\infty$ tends to increase. The difference between the infinity norms of both models is accentuated as the level of CIG exceeds 35%. This in turn means that the transients of the system simulated through the QPC-based model are considerably different to those obtained through its counterpart based on DPC.

C. Sensitivity Analysis

The modal analysis has shown that the critical modes of the system based on QPC-models are $\mathrm{M1_{QPC}}$ and $\mathrm{M2_{QPC}}$. In the case of DPC-based models, there are no critical modes. However, we consider for this analysis the mode $\mathrm{M1_{DPC}}$ because it is the mode for which its corresponding eigenvalue is relatively close to the eigenvalues pertaining to $\mathrm{M1_{QPC}}$ and $\mathrm{M2_{QPC}}$. The sensitivity analysis is carried out for different parameters of the CIG control. Specifically, we present the effects of changing the PLL control parameters of both CIG1 and CIG3. To do this,

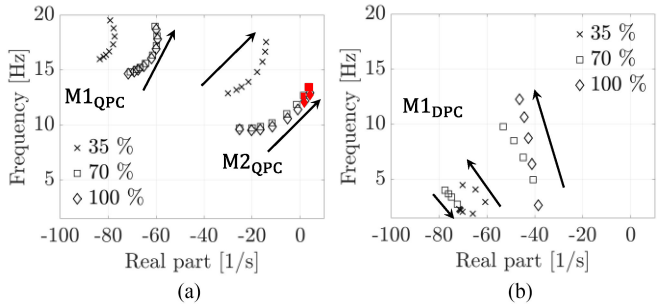

Fig. 9. Eigenvalue loci of the modes related to the CIG control for PLL bandwidth between 2 and 30 Hz; a) QPC-based model, b) DPC-based model.

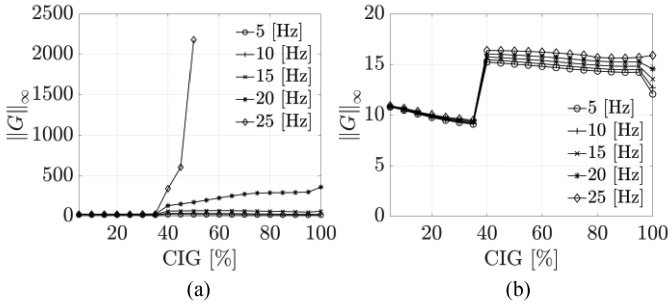

Fig. 10. $\|\boldsymbol{G}\|_\infty$ as a function of CIG penetration level and different PLL bandwidth frequencies; a) QPC-based model, b) DPC-based model.

the frequency bandwidth of the PLL is modified between 2 Hz and 30 Hz, which are typical values [39], [44].

The impacts of the different PLL bandwidths on the eigenvalues of interest at 35%, 70%, and 100% of CIG are shown in Fig. 9. The system modeled using the QPC approach becomes less damped or even unstable as the PLL bandwidth and the CIG level increase. Fig. 9a shows that the eigenvalue associated with the mode $\mathrm{M2_{QPC}}$ is close to the right half complex plane. More precisely, the instability appears for PLL bandwidths above 25 Hz and penetration levels in access of 70%. The unstable modes are highlighted in red in Fig. 9a. In the case of DPC-based models, the effect on the eigenvalue of $\mathrm{M1_{DPC}}$ is shown in Fig. 9b. As the PLL bandwidth increases, the mode $\mathrm{M1_{DPC}}$ always remains well damped, taking a minimum damping of 51%. For this case, the small-signal model is always stable when using DPC regardless of the PLL bandwidth and the CIG level.

Fig. 10 gives the H-infinity norm $\|\boldsymbol{G}\|_\infty$ for different CIG levels and PLL bandwidths. According to Fig. 10a, for QPC-based model, as the PLL bandwidth increases, entailing a faster PLL response, the $\|\boldsymbol{G}\|_\infty$ also increases with the level of CIG. For PLL bandwidths higher than 20 Hz, the models based on QPC suggest instability at high levels of CIG. On the other hand, for the DPC-based model, Fig. 10b reveals no significant variations in the $\|\boldsymbol{G}\|_\infty$ for different levels of CIG and PLL designs. This is consistent with Fig. 10b, showing that the system is always stable when a DPC-based model is used. The visible differences in the $\|\boldsymbol{G}\|_\infty$ of both models point to inaccurate transient simulations using QPC at high CIG levels.

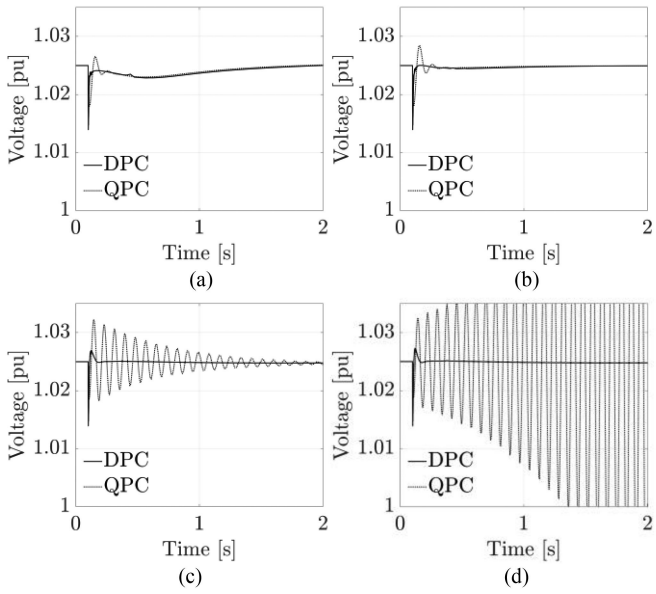

Fig. 11. Terminal voltage at bus B1 for 70% of CIG; a) 2 Hz, b) 5 Hz, c) 20 Hz, d) 25 Hz.

D. Validation Through Time Domain Simulation

The obtained results are now verified by time domain simulations using DPC, QPC, and EMT models. For EMT simulations, PSCAD is used because is a professionally respected representative of the EMT modeling family. A step decreases of 5% in the active power reference of the CIG connected at bus B1 is considered. Simulations are performed for PLL bandwidths of 2 Hz, 5 Hz, 20 Hz, and 25 Hz.

Fig. 11 shows the voltages simulated at bus B1 using DPC and QPC approaches for a CIG level of 70%. According to Fig. 11a and Fig. 11b, when the PLL has a slow response at bandwidths of 2 Hz or 5 Hz, both QPC and DPC models show a similar dynamic behavior. This was expected since the $\|\boldsymbol{G}\|_\infty$ plots of both models do not differ significantly in these cases. However, as the PLL bandwidth is increased to values above 20 Hz, the error obtained by the QPC-based models becomes significant. This can be seen in Fig. 11c and Fig. 11d. In Fig. 11c, when the PLL bandwidth of 20 Hz is used, the oscillation of the voltage is considerably less damped for QPC. Moreover, as shown in Fig. 11d, for a PLL bandwidth of 25 Hz, the system based on QPC becomes unstable. Additionally, we show in Fig. 12 the simulated active power injected to the bus B1. As the PLL bandwidth increases, the oscillation of the active power becomes less damped when the system is modeled using QPC. The previous observations are consistent with the eigenvalue loci depicted in Fig. 9a.

Furthermore, Fig. 13 shows the voltage simulated at B1 using DPC and EMT approaches for a PLL bandwidth of 25 Hz and a CIG level of 100%. At this bandwidth, the simulations of DPC and QPC differ significantly. However, the close-up of Fig. 13 reveals that simulation based on DPC gives a precise envelope of the voltage obtained using EMT models in PSCAD. In Fig. 14, the active power injected to bus B1 for PLL bandwidths of 2 Hz,

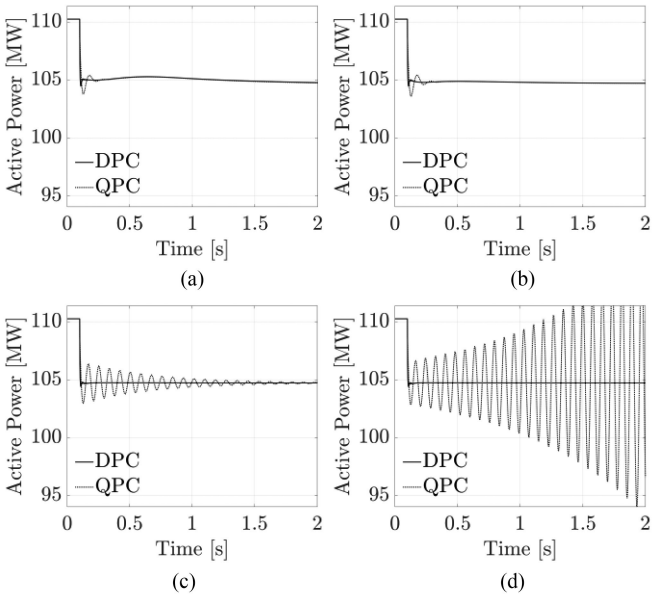

Fig. 12. Active power injected to bus B1 for 70% of CIG; a) 2 Hz, b) 5 Hz, c) 20 Hz, d) 25 Hz.

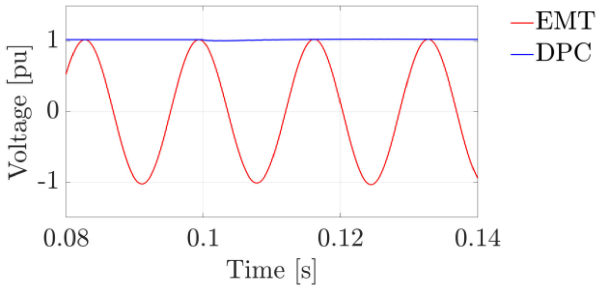

Fig. 13. Terminal voltage at bus B1 for 100% of CIG and PLL bandwidth of 25 Hz.

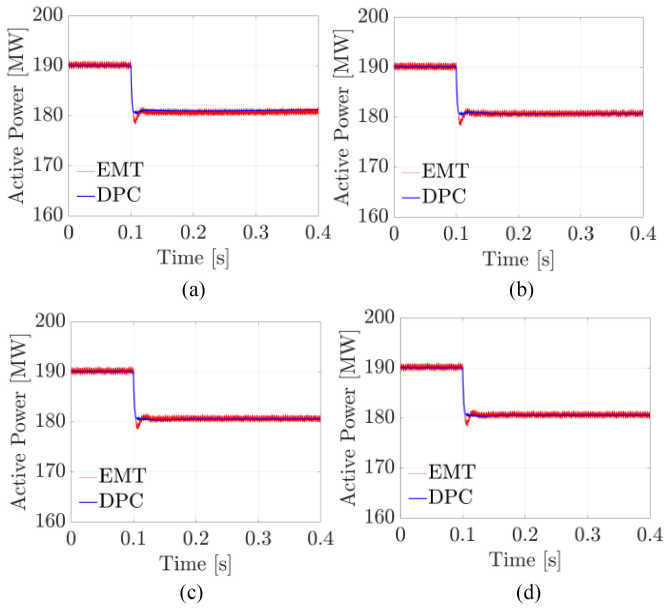

Fig. 14. Active power injected to bus B1 for 70% of CIG; a) 2 Hz, b) 5 Hz, c) 20 Hz, d) 25 Hz.

TABLE VI
SUMMARY OF MAIN FINDINGS

Findings	QPC	DPC
Frequency bandwidth of transients wherein the modeling technique is suitable to simulate AC grids	≤ 5 Hz	> 0 Hz
Capability for modeling slow electromechanical transients	High	High
Capability for modeling both electromagnetic and electromechanical transients	-	High
Accuracy in the representation of fast control systems of CIG	Low	High
Accuracy in transient simulations of systems with high CIG penetration levels	Low	High

5 Hz, 20 Hz, and 25 Hz is depicted. It can be seen the high-frequency transients in the active power due to the PWM control. The results obtained from DPC-based models match very closely with those obtained from EMT simulations using PSCAD. There are no significant differences, regardless of the PLL bandwidth used in these cases. This was expected since the H-infinity norms $\|\boldsymbol{G}\|_\infty$ of DPC models shown in Fig.10b are similar for those PLL bandwidths.

The transient simulations confirm and validate the assessments of the stages 2, 3, and 4 of Fig. 3. The fast response of the CIG control systems leads to a decrease in the accuracy of QPC models in transient simulation. This in turn makes the use of QPC unsuitable for generic stability assessment of power systems with increasing and significant CIG levels.

In Table VI, we summarize some of the main findings obtained from this analysis. In general, it was observed that QPC models should not be used for transients with a frequency range above 5 Hz. DPC models in turn have shown to be practical for simulating higher frequencies, even in power systems with very high CIG penetration levels.

VI. CONCLUSION

In this paper, a comparative analysis of quasi-static and dynamic phasor calculus was performed considering penetration levels of CIG up to 100%. The analysis offers novel insight and fosters the understanding of power system modeling for the purpose of stability assessments of systems with a significant share of CIG. Knowing that the fast phenomena of CIG and of the network itself affect the dynamic behavior of the system, we determined how the extended bandwidth of relevant transients modifies the validity range of models based on quasi-static phasors. To accomplish this, a novel methodology for a systematic analysis of the underlying modeling framework was developed.

Based on the obtained results, the accuracy of quasi-static phasor calculus decreases in the cases of high CIG levels. In these cases, the bandwidth of relevant transients for stability is to be extended for covering both electromagnetic and electromechanical transients, with oscillation frequencies beyond $f_* \approx 5$ Hz. Hence, the relevant oscillation frequencies for stability studies move outside the range of 0.1 Hz to 5 Hz, which is a relevant bandwidth for stability analysis of systems dominated by synchronous generators. Since fast transients with oscillation

frequencies beyond 5 Hz become relevant for stability analysis, the electromagnetic phenomena related to the network and fast response devices cannot be neglected.

Furthermore, control loops like those for the phase locked loop have an impact on the system such that electromagnetic transients on the grid side cannot be ignored in general. Models based on dynamic phasor calculus can accurately represent such transients and are suitable for assessing the stability in the presence of CIG. Given the strong interest in advancing wind and solar energy, the modeling of power systems based on dynamic phasor calculus is recommended.

REFERENCES

[1] P. Kundur *et al.*, "Definition and classification of power system stability," *IEEE Trans. Power Syst.*, vol. 19, no. 3, pp. 1387–1401, May 2004.

[2] P. W. Sauer and M. A. Pai, in *Power System Dynamics and Stability*. NJ, NJ, USA: Prentice-Hall, 1998.

[3] M. Ilic and J. Zaborszky, in *Dynamics and Control of Large Electric Power Systems*. NY, NY: Wiley-IEEE Press, 2000.

[4] P. Kundur, in *Power System Stability and Control*. NY, NY, USA: McGraw-Hill, 1994.

[5] G. Gross, C. F. Imparato, and P. M. Look, "A tool for the comprehensive analysis of power system dynamic stability," *IEEE Trans. Power Appar. Syst.*, vol. PAS-101, no. 1,, pp. 147–157, Jan. 1982.

[6] I. Erlich, A. Korai, and F. Shewarega, "Control challenges in power systems dominated by converter interfaced generation and transmission technologies," in *Proc. IEEE PES General Meeting*, Chicago, IL 2017.

[7] N. Hatziargyriou *et al.*, "Stability definitions and characterization of dynamic behavior in systems with high penetration of power electronic interfaced technologies," *IEEE PowerEnergy Soc.*, Technical Report, PES-TR77, pp. 1–42, 2020.

[8] M. Paolone *et al.*, "Fundamentals of power systems modelling in the presence of converter-interfaced generation," in *Proc. 21st Power Syst. Comput. Conf. - PSCC2020*, 2020, pp. 1–35.

[9] L. Fan, "Modeling type-4 wind in weak grids," *IEEE Trans. Sustain. Energy*, vol. 10, no. 2, pp. 853–863, Apr. 2019.

[10] L. Fan and Z. Miao, "Wind in weak grids : 4 hz or 30 hz oscillations?," *IEEE Trans. Power Syst.*, vol. 33, no. 5, pp. 5803–5804, Sep. 2018.

[11] H. Liu, X. Xie, and W. Liu, "An oscillatory stability criterion based on the unified dq - frame impedance network model for power systems with high-penetration renewables," *IEEE Trans. Power Syst.*, vol. 33, no. 3, pp. 3472–3485, May. 2018.

[12] H. Liu and X. Xie, "Impedance network modeling and quantitative stability analysis of sub - / Super-synchronous oscillations for large-scale wind power systems," *IEEE Access*, vol. 6, pp. 34431–34438, 2018.

[13] M. Zhao, X. Yuan, J. Hu, and Y. Yan, "Voltage dynamics of current control time-scale in a VSC-connected weak grid," *IEEE Trans. Power Syst.*, vol. 31, no. 4, pp. 2925–2937, Jul. 2016.

[14] W. Du, X. Chen, and H. Wang, "PLL-induced modal resonance of grid-connected PMSGs with the power system electromechanical oscillation modes," *IEEE Trans. Sustain. Energy*, vol. 8, no. 4, pp. 1581–1591, Oct. 2017.

[15] "in *Analytic Research Foundations For the Next-Generation Electric Grid*." The National Academies Press, WA DC, USA, 2016.

[16] M. Parniani and M. Iravani, "Computer analysis of small-signal stability of power systems including network dynamics," *IEE Proc. - Gener. Transm. Distrib.*, vol. 142, no. 6, pp. 613–617, Nov. 1995.

[17] F. Milano, F. Dörfler, G. Hug, D. J. Hill, and G. Verbic, "Foundations and challenges of low-inertia systems," in *Proc. 20th Power Syst. Comput. Conf.*, 2018, pp. 1–25.

[18] J. Matevosyan *et al.*, "Grid-forming inverters: Are they the key for high renewable penetration?," *IEEE Power Energy Mag*, vol. 17, no. 6, pp. 89–98, Nov.-Dec. 2019.

[19] NERC, "Integrating inverter - based resources into low short circuit strength systems - Reliability guideline," 2017.

[20] A. M. Stankovic, B. C. Lesieutre, and T. Aydin, "Modeling and analysis of single-phase induction machines with dynamic phasors," *IEEE Trans. Power Syst.*, vol. 14, no. 1, pp. 9–14, Feb. 1999.

[21] K. Strunz, R. Shintaku, and F. Gao, "Frequency-adaptive network modeling for integrative simulation of natural and envelope waveforms in power systems and circuits," *IEEE Trans. Circuits Syst. I Regul. Pap.*, vol. 53, no. 12, pp. 2788–2803, Dec. 2006.

[22] V. Venkatasubramanian, "Tools for dynamic analysis of the general large power system using time-varying phasors," *Int. J. Electr. Power Energy Syst.*, vol. 16, no. 6, pp. 365–376, 1994.

[23] F. Gao and K. Strunz, "Frequency-adaptive power system modeling for multiscale simulation of transients," *IEEE Trans. Power Syst.*, vol. 24, no. 2, pp. 561–571, May. 2009.

[24] P. Zhang, J. R. Martí, and H. W. Dommel, "Shifted-frequency analysis for EMTP simulation of power-system dynamics," *IEEE Trans. Circuits Syst. I Regul. Pap.*, vol. 57, no. 9, pp. 2564–2574, Sep. 2010.

[25] Z. Shuai, Y. Peng, J. M. Guerrero, Y. Li, and Z. J. Shen, "Transient response analysis of inverter-based microgrids under unbalanced conditions using a dynamic phasor model," *IEEE Trans. Ind. Electron.*, vol. 66, no. 4, pp. 2868–2879, Apr. 2019.

[26] T. Yang, S. Bozhko, G. Asher, and C. I. Hill, "Dynamic phasor modeling of multi-generator variable frequency electrical power systems," *IEEE Trans. Power Syst.*, vol. 31, no. 1, pp. 563–571, Jan. 2016.

[27] Z. Miao, L. Piyasinghe, J. Khazaei, and L. Fan, "Dynamic phasor-based modeling of unbalanced radial distribution systems," *IEEE Trans. Power Syst.*, vol. 30, no. 6, pp. 3102–3109, Nov. 2015.

[28] Y. Xia and K. Strunz, "Multi-scale induction machine model in the phase domain with constant inner impedance," *IEEE Trans. Power Syst.*, pp. 1–13, 2019.

[29] Y. Xia, K. Strunz, Y. Chen, and Y. Song, "Multi-scale modeling and simulation of DFIG-based wind energy conversion system," *IEEE Trans. Energy Convers.*, vol. 35, no. 1, pp. 560–572, 2020.

[30] J. Rupasinghe, S. Filizadeh, and L. Wang, "A dynamic phasor model of an MMC with extended frequency range for EMT simulations," *IEEE J. Emerg. Sel. Top. Power Electron.*, vol. 7, no. 1, pp. 30–40, Mar. 2019.

[31] H. D. Lüke, in *Signalübertragung*, 4th ed.. Berlin, Germany: Springer-Verlag, 1990.

[32] J. R. Winkelman, J. H. Chow, and J. J. Allemong, "Multi-time-scale analysis of a power system," *Automatica*, vol. 16, pp. 35–43, 1980.

[33] S. Ahmed-Zaid, P. W. Sauer, M. A. Pai, and M. K. Sarioglu, "Reduced order modeling of synchronous machines using singular perturbation," *Trans. Circuits Syst.*, vol. 29, no. 11, pp. 782–786, 1982.

[34] "IEEE recommended practice for excitation system models for power system stability studies," *IEEE Stand. 421.5*, 2016.

[35] P. Pourbeik *et al.*, "Dynamic models for turbine-governors in power system studies," *IEEE Power Energy Soc. Tech. Rep. PES -TR1*, 2013.

[36] S. Chiniforoosh *et al.*, "Definitions and applications of dynamic average models for analysis of power systems," *IEEE Trans. Power Deliv.*, vol. 25, no. 4, pp. 2655–2669, 2010.

[37] A. Yazdani *et al.*, "Modeling guidelines and a benchmark for power system simulation studies of three-phase single-stage photovoltaic systems," *IEEE Trans. Power Del.*, vol. 26, no. 2, pp. 1247–1264, Apr. 2011.

[38] A. Yazdani and R. Iravani, in *Voltage-sourced Converters in Power Systems*. Hoboken, NJ, USA: John Wiley & Sons, 2010.

[39] D. Zhang, Y. Wang, J. Hu, S. Ma, Q. He, and Q. Guo, "Impacts of PLL on the DFIG-based WTG's electromechanical response under transient conditions: Analysis and modeling," *CSEE J. Power Energy Syst.*, vol. 2, no. 2, pp. 30–39, 2016.

[40] M. Eremia and M. Shahidehpour, in *Handbook of Electrical Power System Dynamics*. Hoboken, NJ,USA: John Wiley & Sons, 2013.

[41] CIGRE, "Modeling and dynamic behavior of wind generation as it relates to power system control and dynamic performance," in *Proc. CIGRE Work. group C4.601*, 2007.

[42] D. Ramasubramanian, Z. Yu, R. Ayyanar, V. Vittal, and J. Undrill, "Converter model for representing converter interfaced generation in large scale grid simulations," *IEEE Trans. Power Syst.*, vol. 32, no. 1, pp. 765–773, Jan. 2017.

[43] M. R. Iravani, A. s Chandhary, W. J. Giesbrecht, and I. E. Hassan, "Modelling and analysis guidelines for slow transients - Part I torsional oscillations; transient torque; turbine blade vibrations; fast bus transfer," *IEEE Trans. Power Deliv.*, vol. 10, no. 4, pp. 1950–1955, 1995.

[44] L. P. Kunjumuhammed, B. C. Pal, R. Gupta, and K. J. Dyke, "Stability analysis of a PMSG-based large offshore wind farm connected to a VSC-HVDC," *IEEE Trans. Energy Convers.*, vol. 32, no. 3, pp. 1166–1176, Sep. 2017.

[45] L. P. Kunjumuhammed, B. C. Pal, C. Oates, and K. J. Dyke, "Electrical oscillations in wind farm systems: Analysis and insight based on detailed modeling," *IEEE Trans. Sustain. Energy*, vol. 7, no. 1, pp. 51–62, Jan. 2016.
[46] D. Baimel, J. Belikov, J. M. Guerrero, and Y. Levron, "Dynamic modeling of networks, microgrids, and renewable sources in the dq0 reference frame: A survey," *IEEE Access*, vol. 5, pp. 21323–21335, 2017.
[47] B. Pal and B. Chaudhuri, in *Robust Control in Power Systems*. NY, NY: Springer, 2005.
[48] P. Pourbeik *et al.*, "Generic dynamic models for modeling wind power plants and other renewable technologies in large scale power system studies," *IEEE Trans. Energy Convers.*, vol. 32, no. 3, pp. 1108–1116, Sep. 2017.
[49] "Power system models, " 2019. [Online]. Available: www.centroenergia.cl/apppsm.zip
[50] L. Fan, in *Control and Dynamics in Power Systems and Microgrids*. CRC Press, Boca Raton, FL;, 2017.
[51] R. Toscano, in *Structured Controllers For Uncertain Systems: A Stochastic Optimization Approach*. London, UK: Springer London, 2013.
[52] M. Green and D. J. N. Limebeer, *Linear robust control*, Courier Corporation, 2012.
[53] A. M. Gole, R. W. Menzies, H. M. Turanli, and D. A. Woodford, "Improved interfacing of electrical machine models to electromagnetic transients programs," *IEEE Trans. Power Appar. Syst.*, vol. PAS-103, no. 9, pp. 2446–2451, 1984.
[54] P. M. Anderson and A. A. Fouad, in *Power System Control and Stability*, 2nd ed.i. Wiley, Hoboken, NJ, 2003.
[55] S. D'Arco, J. A. Suul, and O. B. Fosso, "A virtual synchronous machine implementation for distributed control of power converters in smartgrids," *Electr. Power Syst. Res.*, vol. 122, pp. 180–197, 2015.
[56] S. Nanou, G. Tsourakis, and C. D. Vournas, "Full-converter wind generator modelling for transient stability studies," in *Proc. IEEE PES Trondheim PowerTech Power Technol. Sustain. Soc. POWERTECH 2011*, pp. 1–7, 2011.
[57] D. Xue and Y. Chen, in *System Simulation Techniques With MATLAB and Simulink*, 1st ed.it. John Wiley & Sons, 2014.
[58] M. Dreidy, H. Mokhlis, and S. Mekhilef, "Inertia response and frequency control techniques for renewable energy sources: A review," *Renewable Sustain. Energy Rev.*, vol. 69, no. Nov. 2016, pp. 144–155, 2017.

Jorge Vega-Herrera is currently working toward the Ph.D. degree in electrical engineering with the University of Chile, Santiago, Chile. His research interests are modeling and stability of power systems, power systems transients, and renewable generation.

Claudia Rahmann received the Ph.D. degree in electrical engineering from the Institute of Power Systems and Power Economics (IAEW), RWTH Aachen University, Aachen, Germany. She is currently a Professor with the Department of Electrical Engineering, University of Chile, Santiago, Chile. Her main research interests are modeling of electrical power systems, power systems dynamics and stability, distributed generation, along with the integration of wind power and photovoltaic generation into power networks.

Felipe Valencia received the Ph.D. degree in control engineering from the Universidad Nacional de Colombia, Medellín, Colombia. He is currently a Full-Time Researcher with the Department of Electrical Engineering, Solar Energy Research Center, Universidad de Chile, Santiago, Chile. He has been involved in different fields, such as power energy generation, transmission, and distribution systems; transportation; and smart grids.

Kai Strunz is currently a Chair Professor of Sustainable Electric Networks and Sources of Energy, Technische Universität Berlin, Berlin, Germany. He is also a Guest Professor of the Chinese Academy of Science, Beijing, China. He is the Chairman of the IEEE PES Subcommittee on Distributed Energy Resources. In 2012, he was the General and Technical Program Chair of the IEEE PES Innovative Smart Grid Technologies (ISGT) Europe 2012 in Berlin. He received the IEEE PES Prize Paper Award in 2015 and the *Journal of Emerging and Selected Topics in Power Electronics* First Prize Paper Award 2015.